PAPER

Check for updates

Visible light assisted hydrogen generation from complete decomposition of hydrous hydrazine using rhodium modified TiO₂ photocatalysts†

Pawan Kumar,[a,b] Anurag Kumar,[a,b] Clémence Queffélec,[c] Dietrich Gudat,[d] Qi Wang,[e] Suman L. Jain, [iD] *[a] Rabah Boukherroub[f] and Sabine Szunerits [iD] *[f]

Hydrogen is considered to be an ideal energy carrier, which produces only water when combined with oxygen and thus has no detrimental effect on the environment. While the catalytic decomposition of hydrous hydrazine for the production of hydrogen is well explored, little is known about its photocatalytic decomposition. The present paper describes a highly efficient photochemical methodology for the production of hydrogen through the decomposition of aqueous hydrazine using titanium dioxide nanoparticles modified with a Rh(I) coordinated catechol phosphane ligand (TiO₂–Rh) as a photocatalyst under visible light irradiation. After 12 h of visible light irradiation, the hydrogen yield was 413 µmol g⁻¹ cat with a hydrogen evolution rate of 34.4 µmol g⁻¹ cat h⁻¹. Unmodified TiO₂ nanoparticles offered a hydrogen yield of 83 µmol g⁻¹ cat and a hydrogen evolution rate of only 6.9 µmol g⁻¹ cat h⁻¹. The developed photocatalyst was robust under the experimental conditions and could be efficiently reused for five subsequent runs without any significant change in its activity. The higher stability of the photocatalyst is attributed to the covalent attachment of the Rh complex, whereas the higher activity is believed to be due to the synergistic mechanism that resulted in better electron transfer from the Rh complex to the conduction band of TiO₂.

Introduction

Hydrogen is considered to be an ideal, environmentally safer and clean energy carrier which can decrease the environmental pollution caused by the use of fossil fuels.[1] The major limitation in using hydrogen as an energy carrier is, however, related to its high mass to volume ratio making its storage in compressed or liquid form very difficult. The development of safer and efficient approaches for the storage of hydrogen has consequently become a subject of prime importance in recent decades. Despite significant progress in this area, the effective storage of hydrogen still remains a challenging issue. So far, a large number of solid materials including BN adducts such as ammonia borane[2] and hydrazine-borane[3] have been explored as potential hydrogen storage materials as they have low molecular weight and high hydrogen density. In addition, various metal hydrides[4] and metal organic frameworks (MOFs)[5] have also been investigated as efficient hydrogen storage materials; these materials liberate, however, hydrogen at elevated temperatures. For practical and technological aspects, hydrogen liberation at a lower temperature is aimed. Chemical hydrogen storage in the form of hydrocarbons and oxygenated hydrocarbons is important due to their high energy density and transportation, but they produce carbon dioxide as a by-product, a greenhouse gas.

In recent decades, hydrazine monohydrate (NH₂NH₂·H₂O) has been acknowledged as ideal for hydrogen storage due to its hydrogen content being as high as 8.0 wt%, liberating nitrogen as the only by-product. A number of efficient catalysts for the decomposition of hydrazine to hydrogen and nitrogen even at ambient temperature have been reported lately.[6] Rhodium–nickel nanoparticles supported on graphene oxide were used by Wang *et al.* for hydrogen evolution from hydrazine hydrate with 100% selectivity at ambient temperature.[7] Singh *et al.* described a nickel–iridium bimetallic catalyst stabilized with cetyltrimethylammonium bromide (CTAB) for

[a]Chemical Sciences Division, CSIR-Indian Institute of Petroleum, Dehradun-248005, India. E-mail: suman@iip.res.in; Fax: +91-135-2660202; Tel: +91-135-2525788
[b]Academy of Scientific and Industrial Research (AcSIR), New Delhi, 110001, India
[c]Chimie Et Interdisciplinarité: Synthèse Analyse Modélisation (CEISAM), Université de Nantes, CNRS, UMR 6230, 2, rue de la Houssinière, BP 92208, 44322 Nantes Cedex 3, France
[d]Institut für Anorganische Chemie, University of Stuttgart, Pfaffenwaldring 55, 70550 Stuttgart, Germany
[e]Key Laboratory for Liquid–Solid Structural Evolution and Processing of Materials, Shandong University, Jinan 250061, China
[f]Univ. Lille, CNRS, Centrale Lille, ISEN, Univ. Valenciennes, UMR 8520 – IEMN, F-59000 Lille, France. E-mail: sabine.szunerits@univ-lille1.fr
†Electronic supplementary information (ESI) available. See DOI: 10.1039/c6pp00432f

the degradation of hydrazine to hydrogen.[8] Tong *et al.* investigated multiwalled carbon nanotube supported iron–boron catalysts (Fe–B/MWCNTs), prepared *via* the chemical reduction of aqueous sodium borohydride with iron chloride, for the degradation of hydrazine hydrate.[9] All these reports are based on the use of expensive catalytic systems, which require tedious synthetic procedures.

Semiconductor based photocatalysts such as TiO_2, ZnO, $InVO_4$, $(Ga_{1-x}Zn_x)(N_{1-x}O_x)$, *etc.* could be interesting alternative materials. These catalysts are widely used for solar light driven photocatalytic degradation of dyes and pollutants, oxidation of volatile organic materials as well as for hydrogen generation and CO_2 reduction.[10] Among them, titania (TiO_2) due to its non-toxic nature, low cost and availability has been most extensively used. Due to its wide band gap of 3.2 eV for the anatase form, TiO_2 absorbs only in the UV region, which accounts for only 5% of the total solar radiation. A number of approaches including doping with metals (Cu, Au, Pt, *etc.*), nonmetals (C, N, S, I, *etc.*) and sensitization with dyes have been suggested to enhance the absorbance in the visible region.[11] The lower quantum efficiency and the premature separation of intermediates from the catalytic surface are the prime factors for poor selectivity of the desired product.

Besides semiconductor based photocatalysts, transition metal complexes based on Ru, Ir, Rh, Pt and Mo complexed with ligands like bipyridines, phosphines, porphyrins, phthalocyanines or others have been identified as reliable photocatalysts for the hydrogen evolution reaction. Brewer *et al.* showed that a mixed-metal Rh^{III}-centered $[\{(bpy)_2Ru(dpp)\}_2RhBr_2]^{5+}$ complex has better light collecting power due to the presence of three metal centres, resulting in higher hydrogen evolution yields.[12] However, such molecular photocatalysts are homogeneous in nature and suffer from non-recyclability and do require sacrificial electron donors. These problems can be overcome by grafting of molecular complexes to photoactive semiconductor supports in which both components can work synergistically. Furthermore, the heterogeneous nature of such photocatalytic platforms provides facile recovery and recycling of the photocatalyst. Recently, Takanabe *et al.* reported that magnesium phthalocyanine immobilized to mpg-C_3N_4 polymeric semiconductor supports *via* π–π interactions provides enhanced hydrogen yields from aqueous solution when compared to the homogeneous analogue.[13] Zhang *et al.* used TiO_2 modified with a binuclear complex of ruthenium $[Ru_2(bpy)_4(BL)](ClO_4)_2$ for photosensitized hydrogen production from water with an apparent quantum yield of 16.5%, without the use of any noble metal co-catalyst.[14] Zhang *et al.* synthesized platinized TiO_2 *via* the grafting of Pt(II) diimine dithiolate complexes onto the surface of TiO_2.[15] The developed systems were highly active and achieved hydrogen yield from water under visible light with a turnover number between 72–84. However, to the best of our knowledge, currently there has been no report on the photocatalytic hydrogen evolution from hydrazine hydrate.

In continuation of our ongoing research on photocatalytic transformations,[16] herein we report for the first time, visible
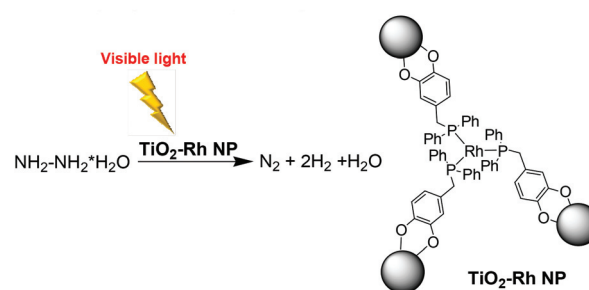
Fig. 1 Schematic illustration of photocatalytic hydrogen evolution from hydrazine catalysed by TiO_2–Rh NPs under visible light illumination.

light assisted hydrogen generation from hydrazine hydrate using Rh^{1+} modified TiO_2 nanoparticles (TiO_2–Rh NPs) as visible light photocatalysts (Fig. 1).

Results and discussion

Synthesis of rhodium chelated TiO_2 nanoparticles (TiO_2–Rh NPs) and characterization

The strategy for the immobilization of the rhodium/ligand **1** complex onto TiO_2 NPs is depicted in Fig. 2. After the formation of TiO_2 nanoparticles by hydrolysis of Ti(O–iPr)$_4$ under basic conditions, immobilization of ligand **1** is performed through the interaction of the catechol ligand with the hydroxyl groups of TiO_2 and subsequent complexation of the phosphane groups with $[Rh(COD)Cl]_2$, resulting in TiO_2–Rh NPs. Indeed, it is well known that catechols and their derivatives can self-assemble rapidly on TiO_2 NPs by replacement of the surface hydroxyl groups of TiO_2 NPs by the deprotonated catechol ligands.[17]

The TEM images of the TiO_2–Rh NPs are shown in Fig. 2b and can be seen in the form of black spots with a size between 25 and 50 nm. Larger clusters are ascribed to the agglomerated TiO_2 particles. The size of the agglomerates is about ten times higher than the primary particle sizes. The lattice fringes with a spacing of 3.5 Å are assigned to anatase TiO_2 (101). The associated SAED pattern (Fig. 2c), obtained from the nanoparticles shown in Fig. 2b, confirms the presence of tetragonal anatase TiO_2. A comparison between the interplanar distances of the first size rings calculated from the SAED pattern and the tabulated ones for the TiO_2 anatase crystallographic structure reveals a high degree of consistency (Table 1). The first six rings are assigned to the (101), (004), (200), (211) and (204) reflections of the anatase phase.

XPS analysis was used to confirm the successful integration of the ligands onto the TiO_2 NPs. The XPS survey spectrum displays bands at 133 eV (P_{2p}, 3.6 at%), 310 eV (Rh_{3d}, 1.1 at%), 285 eV (C_{1s}, 47.8 at%), 459 eV (Ti_{2p}, 9.7 at%) and 527 eV (O_{1s}, 38.0 at%), in accordance with the expected chemical composition (Table S1†). The measured P/Rh ratio (3.2) is close to the value expected for the formation of a Wilkinson-type complex (P3/Rh), suggesting that the majority of phosphine groups are

This journal is © The Royal Society of Chemistry and Owner Societies 2017

Photochem. Photobiol. Sci., 2017, **16**, 1036–1042 | **1037**
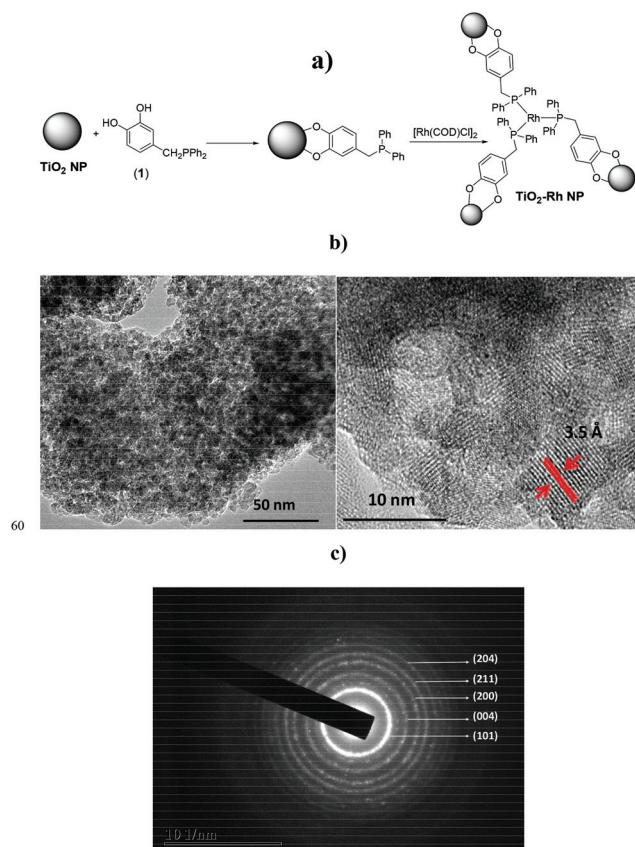
Fig. 2 (a) Formation of Rh(I)-modified TiO_2 nanoparticles, (b) TEM images of TiO_2–Rh NPs. The high resolution TEM image shows lattice fringes of the 3.5 nm interlayer spacing and (c) SAED pattern of TiO_2–Rh NPs.

Table 1 Interplanar distances for TiO_2–Rh NPs deduced from the SAED patterns and compared to the expected ones for an ideal anatase phase

Interplanar distance from SAED pattern (Å)	3.551	2.373	1.920	1.920
Theoretical distance from the anatase phase (Å)	3.520	2.378	1.892	1.892
Corresponding Miller indices	(101)	(004)	(200)	(204)

coordinated with Rh. Fig. 3a depicts the C_{1s} high resolution spectrum. It can be deconvoluted into two bands at 284.5 eV due to the aromatic catechol ring and phenyl groups of the phosphane ligand (1) and another at 288.8 eV due to the C–O–Ti linkage.

Fig. 3b shows the Ti_{2p} high resolution of TiO_2–Rh NPs. The spin–orbit-split $2p_{3/2}$ and $2p_{1/2}$ components can be clearly seen in the Ti_{2p} spectrum at binding energies of 459.0 and 464.0 eV, respectively. The band at 459.0 eV arises from the majority of surface Ti^{4+} ions in accordance with the literature for anatase TiO_2. The binding energy of P_{2p} of the tethered phosphanes is located at 133.0 eV (Fig. 3c), in accordance with the presence of phosphane ligands complexed by rhodium, although the presence of phosphane oxide cannot be ruled out.[18]
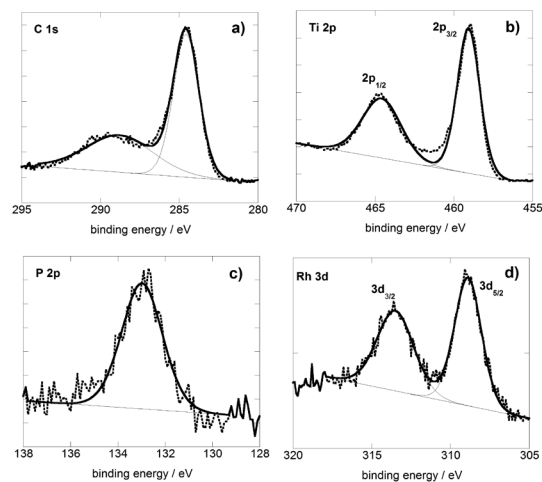
Fig. 3 High resolution XPS spectra of TiO_2–Rh NPs: (a) C_{1s}, (b) Ti_{2p}, (c) P_{2p} and (d) Rh_{3d}.

The high resolution spectrum of Rh_{3d} shows two peaks at 308.9 and 313.6 eV due to $3d_{5/2}$ and $3d_{3/2}$ contributions, respectively (Fig. 3d). The binding energy of the $3d_{5/2}$ component is typical of rhodium(I), indicating that the formal oxidation state of the metal is unchanged after heterogenization and that rhodium nanoparticles were not formed.[19]

The UV-Vis spectrum of TiO_2–Rh NPs (Fig. 4) exhibits strong absorption in the UV region (below 380 nm), being comparable to that of unmodified TiO_2 NPs. However, the presence of the Rh complex results in an additional absorption band in the visible region due to MLCT transition of the rhodium complex and an extended absorption tail up to 625 nm which confirms that the TiO_2–Rh NP catalyst can absorb in the visible region.[20]

Photocatalytic activity

The synthesized TiO_2 and TiO_2–Rh photocatalysts were tested for the hydrogen evolution reaction from hydrazine under visible light. A reaction mixture of photocatalysts and degassed hydrazine hydrate was irradiated in a cylindrical vessel by
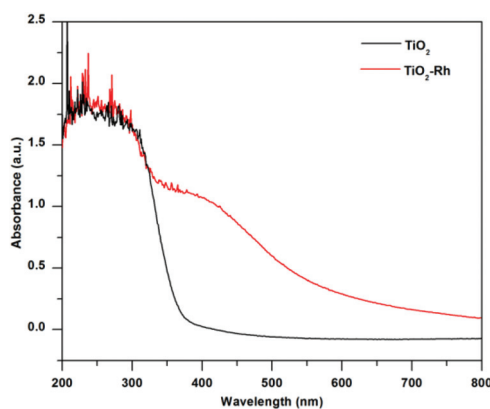
Fig. 4 UV-Vis spectra of TiO_2 NPs (black) and TiO_2–Rh NPs (red).

1038 | *Photochem. Photobiol. Sci.*, 2017, **16**, 1036–1042

This journal is © The Royal Society of Chemistry and Owner Societies 2017

using a 20 W white LED light. The reaction progress was monitored by analyzing the gas samples collected every 2 h of irradiation by using GC-FID and GC-TCD. For quantitative determination of hydrogen, a standard gaseous mixture (refinery gas test sample (P/N-5080-8755) supplied by Agilent Technologies) was injected into GC-FID and GC-TCD and the obtained peak area was correlated with the reaction mixture. Gaseous analysis showed the formation of hydrogen and nitrogen as the products of photocatalytic degradation (oxidation) of hydrazine. The performance of the photocatalysts was plotted in terms of hydrogen yield (in micromoles) *vs.* time as shown in Fig. 5. The yield of hydrogen by using TiO_2–Rh and TiO_2 as photocatalysts under identical conditions was determined to be 413 and 83 $\mu mol\ g^{-1}$ cat, respectively, after 12 h of vis-irradiation. The hydrogen formation rates R_{H_2} for Rh–TiO_2 and TiO_2 were 42.0 and 6.9 $\mu mol\ g^{-1}$ cat h^{-1}, respectively, after 12 h. It is important to mention that on the basis of gaseous phase analysis by GC-TCD, the possibility of NH_3 production cannot be ruled out as NH_3 is highly soluble in water and therefore may not be present in the gaseous mixture. Hence, to confirm the formation of NH_3 during the photoreaction, we performed ^{15}N NMR analysis of hydrazine solution before and after the reaction using CD_3NO_2 as the external reference (Fig. S2†). As can be seen in Fig S2 (ESI†), a very small peak at δ (approx. 376 ppm) appeared which confirmed the formation of NH_3 during the photoreaction. However, the intensity of the peak is very low, indicating the formation of a very low amount of ammonia in the present methodology. Since the amount of ammonia was very low, it was difficult to determine the selectivity of the reaction for N_2/H_2 *vs.* N_2/NH_3. However, the absence of hydrazine at the end of the reaction confirmed the complete decomposition of hydrazine to give nitrogen and hydrogen gases selectively along with the formation of ammonia in very minute amounts.

Two blank experiments, one in the dark in the presence of a photocatalyst and the other under light irradiation without a photocatalyst, were performed to confirm that the reaction was photocatalytic in nature. In both cases, no trace of hydrogen even after a long time of irradiation was observed, which confirmed the photocatalytic nature of the reaction. These results are summarized in Fig. 5a. Further, we have calculated the quantity of nitrogen evolved for checking the stoichiometric performance of the photocatalytic reaction. A standard sample of nitrogen (pure nitrogen) was injected into the GC system to determine the quantitative yield of nitrogen. After 12 h of visible light irradiation, the yield of nitrogen was found to be 194 $\mu mol\ g^{-1}$ cat. The calculated ratio of hydrogen to nitrogen (H : N) was (2.12 : 1), which was near to the theoretical ratio 2 : 1 and thus confirmed that the derived hydrogen was generated from the decomposition of hydrazine.
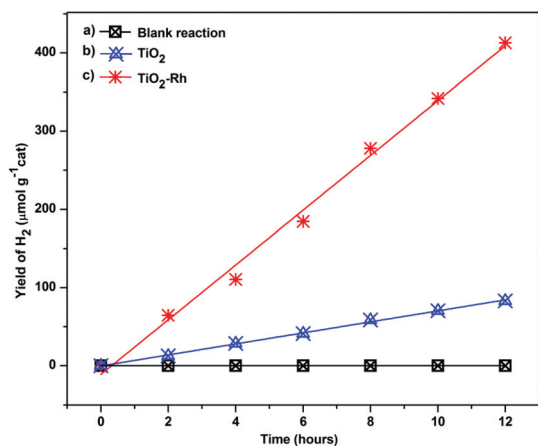
Further, to check the formation of Rh nanoparticles during the reaction, we recovered the catalyst after the photoreaction and analyzed by HR-TEM (Fig. S1†). The HR-TEM image clearly indicated that no Rh particles were formed on the surface of TiO_2 during the photoreaction, and hence it can be concluded that the reaction was truly catalyzed by TiO_2–Rh nanoparticles instead of Rh nanoparticles.[21]

To establish the stability of the photocatalyst, recycling experiments were performed under the described experimental conditions. After completion of the reaction, the photocatalyst was easily recovered by centrifugation, washed with ethanol and reused for subsequent runs. The results of these experiments are summarized in Fig. 6. As shown in Fig. 6, the recovered photocatalyst was found to be quite effective as after five recycling experiments the yield of hydrogen was found to be 384 $\mu mol\ g^{-1}$ cat. However, photoactivity decreased slightly in the subsequent run, which was probably due to the leaching of the Rh complex from the surface of TiO_2. In order to confirm the leaching, the recovered photocatalyst after the fifth run was analyzed by ICP-AES; the value of the Rh metal after the fifth cycle was 0.14 wt% which was slightly lower in comparison with the fresh one (0.16 wt%). This confirms that the activity loss was due to Rh complex's leaching from the surface of TiO_2.

Fig. 5 Graph of hydrogen evolution *vs.* time by using (a) a blank reaction in the dark and without catalyst, (b) TiO_2 and (c) TiO_2–Rh photocatalysts.
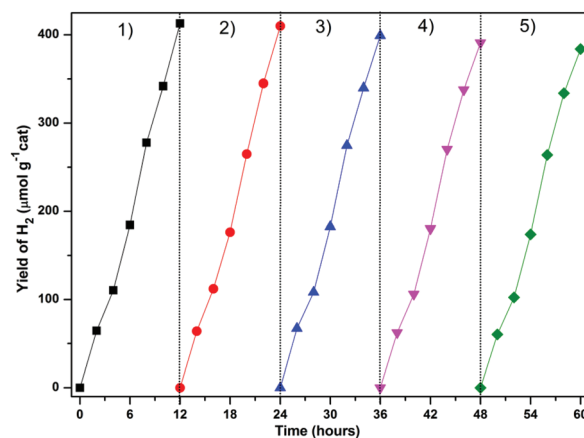
Fig. 6 Results of the photocatalytic stability of catalysts for photocatalytic hydrogen evolution during five cycles.

This journal is © The Royal Society of Chemistry and Owner Societies 2017

Photochem. Photobiol. Sci., 2017, **16**, 1036–1042 | **1039**

If the photogenerated holes at the valence band of TiO_2 were the primary species responsible for the oxidation of hydrazine, then addition of a hole scavenger should hamper the progress of the reaction, which will be a direct indication of the involvement of holes in the oxidation of hydrazine.[22] To evaluate the role of holes produced in the process for the photochemical oxidation of hydrazine, we have carried out the photo-reaction by using a TiO_2–Rh photocatalyst, in the presence of EDTA·2Na as a hole scavenger under identical reaction conditions. The quantitative estimation of evolved hydrogen was done using GC-FID every 2 h. It can be seen from Fig. 7 that after the addition of EDTA·2Na the yield of hydrogen was reduced to 136 μmol g^{-1} cat after 12 h in comparison with that obtained without any hole scavenger (413 μmol g^{-1} cat). This suggests that the oxidation of hydrazine hydrate takes place at the valence band by photogenerated holes.

A plausible mechanism was proposed for defining better photocatalytic performance of the synthesized photocatalyst. The reduction potential required for hydrogen evolution (H^+/H_2) is 0.00 V at pH = 0; however, −0.41 V overpotential is needed for the production of hydrogen in aqueous solutions (at pH = 7).[23] The position of the conduction band of TiO_2 was negative enough (−0.45 V) to promote the reduction of hydrogen. However, the position of the valence band was positive enough to oxidize hydrazine to generate the required protons and electrons.[24] However, due to its wide band gap, TiO_2 cannot absorb in visible light and therefore cannot produce electron–hole pairs. However, due to the presence of some defects, it can absorb a small part of visible light due to the reduction of the band gap.[25] Hence, unmodified TiO_2 afforded very poor yield of hydrogen (83 μmol g^{-1} cat) under visible light irradiation. After immobilization of the Rh complex to the TiO_2 support, the visible light absorbance was increased due to the absorbance of the Rh complex in the visible region. After absorption of visible light, the Rh complex becomes excited and transfers electrons from the HOMO to the LUMO *via* MLCT transition. These electrons can directly transfer to the conduction band of TiO_2 (Scheme 1).[26] The resulting positively charged
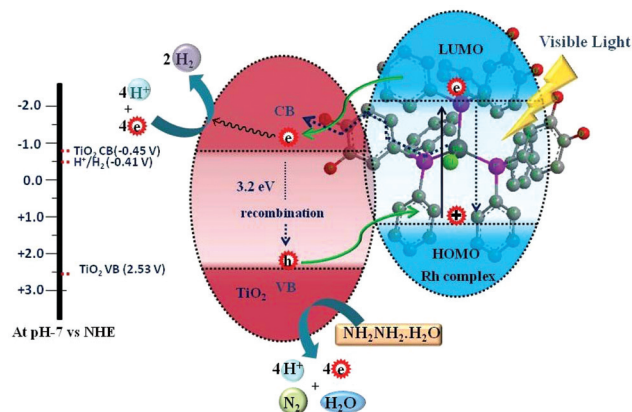
Scheme 1 Mechanism of hydrogen evolution from hydrazine over the TiO_2–Rh catalyst.

Rh complex returns back to its initial state by taking electrons derived from the oxidation of hydrazine at the valence band of TiO_2. The electrons are transferred through the conjugated network from the phosphine ligand to TiO_2. The protons derived from the oxidation of hydrazine are reduced at the conduction band by taking photo-generated electrons (Scheme 1).

Conclusions

The present study demonstrates the first report on the photocatalytic hydrogen generation from the decomposition of hydrazine hydrate using rhodium complex modified TiO_2 under visible light irradiation. After 12 h of visible light irradiation, the yield of hydrogen by using a TiO_2–Rh catalyst was 413 μmol g^{-1} cat, which was much higher than that by bare TiO_2 (83 μmol g^{-1} cat). The covalent immobilization of the rhodium complex to the semiconductor TiO_2 support prevented the leaching and the recovered photocatalyst could be recycled efficiently for five runs without any detectable loss in its activity. The higher photocatalytic performance of TiO_2–Rh was assumed to be due to the synergistic effect of both components which allowed better electron transfer from the excited rhodium complex to the conduction band of TiO_2.

Experimental

Materials

Titanium tetraisopropoxide, chloro(1,5-cyclooctadiene)-rhodium(I) dimer ([Rh(COD)Cl]$_2$), sodium hydroxide (NaOH), hydrazine monohydrate (50–60%) and HPLC grade solvents were purchased from Aldrich and were used as received unless otherwise indicated. Phosphane ligand (**1**) was prepared as reported earlier.[27]

Techniques used

Transmission electron microscopy (TEM) images were recorded on a JEOL JEM-2011 electron microscope operated at an accelerating voltage of 200 kV.
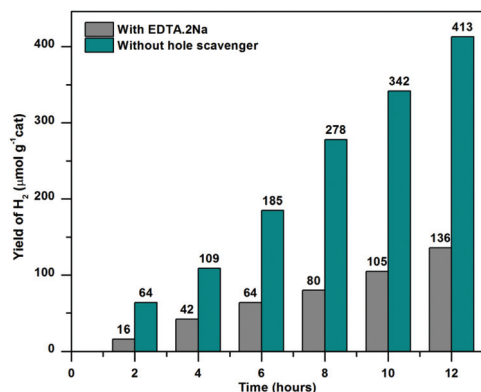
Fig. 7 Photocatalytic hydrogen evolution from hydrazine by using a TiO_2–Rh photocatalyst with EDTA·2Na hole scavenger (grey), and without hole scavenger (green).

X-ray photoelectron spectroscopy (XPS) measurements were performed with an ESCALAB 220 XL spectrometer from Vacuum Generators featuring a monochromatic Al Kα X-ray source (1486.6 eV) and a spherical energy analyzer operated in the CAE (constant analyzer energy) mode (CAE = 100 eV for survey spectra and CAE = 40 eV for high-resolution spectra), using the electromagnetic lens mode. No flood gun source was needed due to the conducting character of the substrates. The angle between the incident X-rays and the analyzer is 58°. The detection angle of the photoelectrons is 30°.

Solid-state magic angle spinning (MAS) NMR experiments were performed on a Bruker Advance spectrometer operating at 7.0 T (^{1}H and ^{31}P Larmor frequencies of 300 and 121.5 MHz, respectively) using a 4 mm double-resonance MAS probe and a spinning frequency of 14 kHz. $\{^1H\}8$-^{31}P cross-polarization (CP). MAS spectra were recorded at a spinning frequency of 14 kHz with ^{1}H and ^{31}P nutation frequencies of 57 and 43 kHz during the CP time of 1 ms. 55 740 transients were accumulated with a recycle delay of 1 s and ^{1}H SPINAL-64 decoupling (radio-frequency field strength of 70 kHz) was applied during signal acquisition.[28]

UV-Vis spectra of solid TiO_2 NP and TiO_2–Rh NP samples were collected on a PerkinElmer lambda-19 UV-VIS-NIR spectrophotometer using a 10 mm quartz cell, and $BaSO_4$ as the reference.

Preparation of Rh-complexed catechol phosphane modified titanium nanoparticles

All reactions were performed under an inert gas using Schlenk techniques. TiO_2 nanoparticles were fabricated by adding titanium tetraisopropoxide (0.48 mL) and sodium hydroxide (1 M, 0.89 mL) to a water/2-propanol mixture (1 : 1, v/v, 12 mL). The mixture was degassed for 15 min and the phosphane ligand (1) (0.1437 mmol, 42.27 mg) was added; the resulting mixture was stirred for 48 h at room temperature. [Rh(COD)Cl]$_2$ (0.0239 mmol, 11.8 mg) was further added and the mixture was stirred for two additional days. The formed particles were precipitated using centrifugation (10 000 rpm, 3 times) and the collected solid was washed with distilled water (3 times) and acetone (3 times) and was finally collected on a filtration membrane. The resulting yellow powder was dried overnight in an oven at 50 °C.

General procedure for hydrogen evolution from hydrazine

Photocatalytic hydrogen evolution from hydrazine hydrate was carried out in a cylindrical Borosil vessel (60 mL, 4.0 cm diameter). At first, the vessel was filled up to 25 mL with hydrazine followed by nitrogen purging to remove dissolved gaseous components. After that, 50 mg of catalyst was added to the vessel and all the remaining gas in the vessel was evacuated with the help of a vacuum pump. The vessel was closed tightly with a rubber septum and then irradiated under visible light by using a 20 W white cold LED flood light (model no. HP-FL-20W-F-Hope LED Opto-Electric Co. Ltd) under stirring. The light intensity on the surface of the vessel was 75 W m^{-2} as measured by using an intensity meter (model: Lumen Lux;

company: Palida, Norway). The progress of the reaction was monitored by collecting the gaseous samples at 2 h intervals by using a needle and analyzing them by GC-TCD and GC-FID (Agilent 7890A GC system) using a capillary column (RGA, refinery gas analyzer) with the following flow rate parameters: H$_2$: 35 mL min^{-1}, air: 350 mL min^{-1}, makeup flow: 27 mL min^{-1}, for TCD reference flow: 45 mL min^{-1}, helium flow: 2 mL min^{-1} and injector temperature: 220 °C, TCD detector temperature and FID detector temperature: 220 °C. Each time 20 μL of gaseous sample was injected into GC and the yield was determined by injecting the standard gaseous mixture (refinery gas test sample (P/N-5080-8755) 15% v/v hydrogen, pressure 2 bar, volume 1 litre, supplied by Agilent Technologies). In order to confirm that the evolved hydrogen was generated from the decomposition of hydrazine, we also measured the evolved nitrogen. The ratio of nitrogen to hydrogen was determined to confirm the origin of evolved hydrogen from the decomposition of hydrazine. Controlled reactions in the dark using a photocatalyst and in light without a photocatalyst did not produce hydrogen even after a prolonged time under identical conditions. These results confirmed that hydrogen was produced from the photocatalytic degradation of hydrazine. To establish the superiority of the TiO_2–Rh NP photocatalyst, a blank experiment using unmodified TiO_2 was also conducted under identical conditions.

Notes and references

1 (*a*) M. Felderhoff, C. Weidenthaler, R. V. Helmolt and U. Eberle, *Phys. Chem. Chem. Phys.*, 2007, **9**, 2643–2653; (*b*) A. E. Atabani, A. S. Silitonga, I. A. Badruddin, T. M. I. Mahlia, H. H. Masjuki and S. Mekhilef, *Renewable Sustainable Energy Rev.*, 2012, **16**, 2070–2093.

2 (*a*) M. Zahmakiran and S. Ozkar, *Appl. Catal., B*, 2009, **89**, 104–110; (*b*) Y. Yamada, K. Yano, Q. Xu and S. Fukuzumi, *J. Phys. Chem. C*, 2010, **114**, 16456–16462.

3 S. Karahan, M. Zahmakıran and S. Ozkar, *Int. J. Hydrogen Energy*, 2011, **36**, 4958–4966.

4 (*a*) S. Orimo, Y. Nakamori, J. R. Eliseo, A. Zuttel and C. M. Jensen, *Chem. Rev.*, 2007, **107**, 4111–4132; (*b*) L. Schlapbach and A. Zuttel, *Nature*, 2001, **414**, 353–358.

5 (*a*) A. W. C. van den Berg and C. O. Aren, *Chem. Commun.*, 2008, 668–681; (*b*) N. L. Rosi, J. Eckert, M. Eddaoudi,

This journal is © The Royal Society of Chemistry and Owner Societies 2017

Photochem. Photobiol. Sci., 2017, **16**, 1036–1042 | **1041**

D. T. Vodak, J. Kim, M. O′Keeffe and O. M. Yaghi, *Science*, 2003, **300**, 1127–1129.

6 (*a*) H.-L. Jiang, S. K. Singh, J.-M. Yan, X.-B. Zhang and Q. Xu, *ChemSusChem*, 2010, **3**, 541–549; (*b*) B. Zhao, J. Song, R. Ran and Z. Shao, *Int. J. Hydrogen Energy*, 2012, **37**, 1133–1139; (*c*) L. He, B. Liang, L. Li, X. Yang, Y. Huang, A. Wang, X. Wang and T. Zhang, *ACS Catal.*, 2015, **5**, 1623–1628.

7 J. Wang, X.-B. Zhang, Z.-L. Wang, L.-M. Wang and Y. Zhang, *Energy Environ. Sci.*, 2012, **5**, 6885.

8 S. K. Singh and Q. Xu, *Chem. Commun.*, 2010, **46**, 6545–6547.

9 D. G. Tong, W. Chu, P. Wu, G. F. Gua and L. Zhang, *J. Mater. Chem. A*, 2013, **1**, 358–366.

10 (*a*) X. Zong, C. Sun, H. Yu, Z. G. Chen, Z. Xing, D. Ye, G. Q. Lu, X. Li and L. Wang, *J. Phys. Chem. C*, 2013, **117**, 4937–4942; (*b*) S. Navalón, A. Dhakshinamoorthy, M. Álvaro and H. Garcia, *ChemSusChem*, 2013, **6**, 562–577; (*c*) K. A. S. Fernando, S. Sahu, Y. Liu, W. K. Lewis, E. A. Guliants, A. Jafariyan, P. Wang, C. E. Bunker and Y.-P. Sun, *ACS Appl. Mater. Interfaces*, 2015, **7**, 8363–8376.

11 (*a*) R. Marschalla and L. Wang, *Catal. Today*, 2014, **225**, 111–135; (*b*) Y. Lia, W. N. Wang, Z. Zhan, M. H. Woo, C. Y. Wu and P. Biswas, *Appl. Catal., B*, 2010, **100**, 386–392; (*c*) I. H. Tseng, W. C. Chang and J. C. S. Wu, *Appl. Catal., B*, 2002, **37**, 37–48; (*d*) Q. Zhang, Y. Li, E. A. Ackerman, M. G. Josifovska and H. Li, *Appl. Catal., A*, 2011, **400**, 195–202; (*e*) Z. Zhang, Z. Wang, S.-W. Cao and C. Xue, *J. Phys. Chem. C*, 2013, **117**, 25939–25947; (*f*) S. G. Kumar and L. G. Devi, *J. Phys. Chem. A*, 2011, **115**, 13211–13241.

12 S. M. Arachchige, J. Brown and K. J. Brewer, *J. Photochem. Photobiol., A*, 2008, **197**, 13–17.

13 K. Takanabe, K. Kamata, X. Wang, M. Antonietti, J. Kubota and K. Domen, *Phys. Chem. Chem. Phys.*, 2010, **12**, 13020–13025.

14 X. Zhang, U. Veikko, J. Mao, P. Cai and T. Peng, *Chem. – Eur. J.*, 2012, **18**, 12103–12118.

15 J. Zhang, P. Du, J. Schneider, P. Jarosz and R. Eisenberg, *J. Am. Chem. Soc.*, 2007, **129**, 7726–7727.

16 (*a*) H. Maaoui, P. Kumar, A. Kumar, G.-H. Pan, R. Chtourou, S. Szunerits, R. Boukherroub and S. L. Jain, *Photochem. Photobiol. Sci.*, 2016, **15**, 1282–1288; (*b*) P. Kumar, C. Joshi, N. Labhsetwar, R. Boukherroub and S. L. Jain, *Nanoscale*, 2015, **7**, 15258–15267; (*c*) P. Kumar, H. P. Mungse, S. Cordier, R. Boukherroub, O. P. Khatri and S. L. Jain, *Carbon*, 2015, **94**, 91–100.

17 (*a*) C. Xu, K. Xu, H. Gu, R. Zheng, H. Liu, X. Zhang, *et al.*, *J. Am. Chem. Soc.*, 2004, **126**, 9938–9939; (*b*) Q. Ye, F. Zhou and W. Liu, *Chem. Soc. Rev.*, 2011, **40**, 4244–4258.

18 C. C. Gheorghiu, B. F. Machado, C. Salinas-Martinez de Lecea, M. Gouygou, M. C. Roman-Martinez and P. Serp, *Dalton Trans.*, 2014, **43**, 7455–7463.

19 C. C. Gheorghiu, B. F. Machado, C. Salinas-Martinez de Lecea, M. Gouygou, M. C. Roman-Martinez and P. Serp, *Dalton Trans.*, 2014, **43**, 7455–7463.

20 D. W. Thompson, A. Ito and T. J. Meyer, *Pure Appl. Chem.*, 2013, **85**, 1257–1305.

21 S. K. Singh, X.-B. Zhang and Q. Xu, *J. Am. Chem. Soc.*, 2009, **131**, 9894–9895.

22 (*a*) Y. Liang, S. Lin, L. Liu, J. Hu and W. Cui, *Appl. Catal., B*, 2015, **164**, 192–203; (*b*) S. Lin, L. Liu, J. Hu, Y. Liang and W. Cui, *Appl. Surf. Sci.*, 2015, **324**, 20–29.

23 A. Naldoni, M. Allieta, S. Santangelo, M. Marelli, F. Fabbri, S. Cappelli, C. L. Bianchi, R. Psaro and V. D. Santo, *J. Am. Chem. Soc.*, 2012, **134**, 7600–7603.

24 (*a*) S. N. Habisreutinger, L. S. Mende and J. K. Stolarczyk, *Angew. Chem., Int. Ed.*, 2013, **52**, 7372–7408; (*b*) J. Yu and J. Ran, *Energy Environ. Sci.*, 2011, **4**, 1364–1371.

25 (*a*) Z. Pei, L. Ding, H. Lin, S. Weng, Z. Zheng, Y. Hou and P. Liu, *J. Mater. Chem. A*, 2013, **1**, 10099–10102; (*b*) J. Wang, Z. Wang, B. Huang, Y. Ma, Y. Liu, X. Qin, X. Zhang and Y. Dai, *ACS Appl. Mater. Interfaces*, 2012, **4**, 4024–4030.

26 (*a*) M. M. Khan, S. A. Ansari, D. Pradhan, M. O. Ansari, D. H. Han, J. Lee and M. H. Cho, *J. Mater. Chem. A*, 2014, **2**, 637–644; (*b*) N. Serpone, *J. Phys. Chem. B*, 2006, **110**, 24287–24293; (*c*) P. Kumar, N. G. Naumov, R. Boukherroub and S. L. Jain, *Appl. Catal., A*, 2015, **499**, 32–38.

27 S. Chikkali and D. Gudat, *Eur. J. Inorg. Chem.*, 2006, 3005–3009.

28 B. M. Fung, A. K. Khitrin and K. Ermolaev, *J. Magn. Reson.*, 2000, **142**, 97–101.